Published in final edited form as:
Dev Cell. 2013 September 16; 26(5): 511–524. doi:10.1016/j.devcel.2013.08.003.

A TRP Channel in the Lysosome Regulates Large Particle Phagocytosis via Focal Exocytosis

Mohammad Samie[1], **Xiang Wang**[1], **Xiaoli Zhang**[1], **Andrew Goschka**[1], **Xinran Li**[1], **Xiping Cheng**[1], **Evan Gregg**[1], **Marlene Azar**[1], **Yue Zhuo**[1], **Abigail Garrity**[1], **Qiong Gao**[1], **Susan Slaugenhaupt**[2], **Jim Pickel**[3], **Sergey N. Zolov**[4], **Lois S. Weisman**[4], **Guy M. Lenk**[5], **Steve Titus**[6], **Marthe Bryant-Genevier**[6], **Noel Southall**[6], **Marugan Juan**[6], **Marc Ferrer**[6], and **Haoxing Xu**[1,*]

[1]Department of Molecular, Cellular, and Developmental Biology, University of Michigan, 3089 Natural Science Building (Kraus), 830 North University, Ann Arbor, MI 48109, USA

[2]Department of Neurology (Genetics), Center for Human Genetic Research, Massachusetts General Hospital/Harvard Medical School, CPZN-5254, 185 Cambridge Street, Boston, MA 02114, USA

[3]NIMH Transgenics, National Institutes of Health, 49 Convent Drive Room B1C25, Bethesda, MD 20892, USA

[4]Department of Cell and Developmental Biology and Life Sciences Institute, University of Michigan, Ann Arbor, Michigan, 48109-2216, USA

[5]Department of Human Genetics, 4909 Buhl, University of Michigan, Ann Arbor, MI 48109, USA

[6]NIH/NCATS/NCGC, 9800 Medical Center Drive, Rockville, MD 20850, USA

Summary

Phagocytosis of large extracellular particles such as apoptotic bodies requires delivery of the intracellular endosomal and lysosomal membranes to form plasmalemmal pseudopods. Here we identified Mucolipin TRP channel 1 (TRPML1) as the key lysosomal Ca^{2+} channel regulating focal exocytosis and phagosome biogenesis. Both particle ingestion and lysosomal exocytosis are inhibited by synthetic TRPML1 blockers, and are defective in macrophages isolated from TRPML1 knockout mice. Furthermore, TRPML1 overexpression and TRPML1 agonists facilitate both lysosomal exocytosis and particle uptake. Using time-lapse confocal imaging and direct patch-clamping of phagosomal membranes, we found that particle binding induces lysosomal $PI(3,5)P_2$ elevation to trigger TRPML1-mediated lysosomal Ca^{2+} release specifically at the site of uptake, rapidly delivering TRPML1-resident lysosomal membranes to nascent phagosomes via lysosomal exocytosis. Thus phagocytic ingestion of large particles activates a phosphoinositide- and Ca^{2+}- dependent exocytosis pathway to provide membranes necessary for pseudopod extension, leading to clearance of senescent and apoptotic cells *in vivo*.

*To whom correspondence should be addressed: haoxingx@umich.edu.

Keywords

Lysosomal exocytosis; Phagocytosis; Phagosome; Membrane trafficking; Ca^{2+} release

Introduction

Macrophages participate in tissue remodeling and cellular clearance by engulfing large extracellular particles, such as apoptotic cells or senescent red blood cells (RBCs), through a highly regulated process called phagocytosis (Flannagan, Jaumouille et al. 2012). Particle binding to specific cell surface receptors such as IgG Fc receptors triggers a cascade of signaling events to rapidly extend the plasma membrane around the particle(s) (Aderem and Underhill 1999). Plasma membrane extensions, called plasmalemmal pseudopods, form phagocytic cups to ingest particles into vacuole-like structures called phagosomes within several minutes after particle binding (Niedergang and Chavrier 2004) (see Fig. 6I). Nascent phagosomes then undergo membrane fusion and fission events, collectively called phagosomal maturation, in a time course of tens of minutes to become phagolysosomes to mediate particle digestion (Aderem and Underhill 1999; Vieira, Botelho et al. 2002). Although a large amount of plasma membrane is internalized during phagocytosis (Aderem and Underhill 1999; Touret, Paroutis et al. 2005), paradoxically, the overall surface area of the phagocytosing cells does not decrease (Braun and Niedergang 2006; Huynh, Kay et al. 2007), and indeed increases significantly before the closing of the phagocytic cups (Holevinsky and Nelson 1998). Consistently, membrane fusion machinery is shown to be required for phagosome formation/biogenesis and efficient phagocytosis (Hackam, Rotstein et al. 1998), and a substantial amount of membrane from intracellular compartments are found to be added to the cell surface at the sites of particle uptake (so called “focal” exocytosis) (Braun, Fraisier et al. 2004; Czibener, Sherer et al. 2006).

Recycling endosomes have been shown as a supply of intracellular membrane for phagosome formation and particle uptake in a Vesicle-Associated Membrane Protein 3 (VAMP3)-dependent manner (Cox, Tseng et al. 1999; Bajno, Peng et al. 2000). More recently lysosomes have been identified as another major source of intracellular membrane required for particle uptake, particularly under high load conditions, i.e., when large (> 5 μm) and/or multiple particles are ingested by a single phagocyte (Huynh, Kay et al. 2007). Under such conditions, lysosomes are involved in the very early steps of phagosome biogenesis/formation, prior to the closing of the phagocytic cups (see Fig. 6I) (Braun, Fraisier et al. 2004; Czibener, Sherer et al. 2006). Fusion of lysosomes with the plasma membrane (lysosomal exocytosis) and the delivery of lysosomal membranes/proteins to the surface of the newly formed phagosomes are observed at the sites of particle ingestion (Swanson, Bushnell et al. 1987; Tapper and Sundler 1995), and manipulations blocking lysosomal exocytosis significantly reduce particle uptake in macrophages (Braun, Fraisier et al. 2004; Czibener, Sherer et al. 2006).

Ca^{2+} is the only known trigger that has been identified for lysosomal exocytosis (Andrews 2000), with Synaptotagmin VII (Syt-VII) being the primary Ca^{2+} sensor in the lysosome (Czibener, Sherer et al. 2006). Vesicle-Associated Membrane Protein 7 (VAMP7), a SNARE protein in the late endosome and lysosome, is required for lysosomal exocytosis (Braun, Fraisier et al. 2004). Consistent with the role of lysosomal exocytosis in particle ingestion, macrophages lacking VAMP7 or Syt VII exhibit defects in both lysosomal exocytosis and particle uptake, but preferentially under high particle loads (Braun, Fraisier et al. 2004; Czibener, Sherer et al. 2006). Intracellular Ca^{2+} ($[Ca^{2+}]_i$) elevation was observed in the vicinity of the particle uptake sites in neutrophils (Theler, Lew et al. 1995; Tapper, Furuya et al. 2002), but not in macrophages (Nunes and Demaurex 2010). However,

preloading cells with the fast membrane-permeant Ca^{2+} chelator BAPTA-AM dramatically reduces lysosomal exocytosis and particle uptake in macrophages (Tapper, Furuya et al. 2002; Czibener, Sherer et al. 2006), suggesting that a small amount of Ca^{2+} release, from non-conventional internal stores that might have escaped detection by using conventional Ca^{2+} imaging methods, may play a crucial role in macrophage phagocytosis. Because the lysosomal lumen is believed to be the main source of Ca^{2+} for Ca^{2+}-dependent vesicular trafficking in the late endocytic pathways (Pryor, Mullock et al. 2000), it is possible that lysosomes themselves provide the Ca^{2+} required for particle-induced exocytosis. However, definitive evidence to support this hypothesis is still lacking, and more importantly, the ion channel(s) responsible for Ca^{2+} release from lysosomes still remains elusive.

Transient Receptor Potential Mucolipin-1 (TRPML1 or ML1) is a member of the TRP cation channel superfamily, and is primarily localized on the lysosome membrane (Cheng, Shen et al. 2010). Human mutations of *TRPML1* cause Mucolipidosis type IV (MLIV), a childhood neurodegenerative disorder with lysosomal trafficking defects at the cellular level (Sun, Goldin et al. 2000; Cheng, Shen et al. 2010). In a *Drosophila* model of MLIV, it has been proposed that the defective clearance of late apoptotic neurons by phagocytes contributes significantly to neurodegeneration (Venkatachalam, Long et al. 2008). By performing patch-clamp recordings directly on lysosomal membranes and by measuring lysosomal Ca^{2+} release using genetically-encoded Ca^{2+} sensors, we have characterized ML1 as a Ca^{2+}-permeable channel on the lysosomal membrane (Dong, Shen et al. 2010; Shen, Wang et al. 2012). ML1 conducts Ca^{2+} from the lysosome lumen into the cytosol and is specifically activated by phosphatidylinositol 3,5-bisphosphate [$PI(3,5)P_2$], a late endosome and lysosome-specific low-abundance phosphoinositide (Dong, Shen et al. 2010). In the current study, using mouse knockouts and synthetic agonists/antagonists of ML1, we investigated the roles of ML1 in phagocytic particle uptake in bone marrow derived macrophages.

Results

Expression of ML1 is necessary for efficient uptake of large particles in mouse macrophages

To study particle uptake/ingestion, we isolated bone marrow macrophages (BMMs) (Chow, Downey et al. 2004) from wild-type (WT) and ML1 knockout (KO) mice (Venugopal, Browning et al. 2007). ML1 KO BMMs contained no detectable level of full-length ML1 transcript, as shown by RT-PCR analysis (Fig. 1A). Consistent with this, direct patch-clamping the endolysosomal membranes (Dong, Cheng et al. 2008) showed that ML-SA1, a membrane-permeable TRPML-specific synthetic agonist (Shen, Wang et al. 2012), and $PI(3,5)P_2$, an endogenous activator of ML1 (Cheng, Shen et al. 2010; Dong, Shen et al. 2010), activated whole-endolysosome ML1-like currents (I_{ML1}) in WT, but not ML1 KO BMMs (Fig. 1B). In contrast, no significant differences were noted in cell morphology, cell size, and CD11b (macrophage-specific surface receptor) immunoreactivity between WT and ML1 KO BMMs (Suppl. fig. S1A).

To investigate the role of ML1 in particle ingestion, WT and ML1 KO BMMs were exposed to IgG-opsonized sheep red blood cells (IgG-RBCs), all about 5 μm in size, for different periods of time (15–90 min; Fig. 1C). IgG-RBC uptake was quantified from at least 150 BMMs per time point for each genotype; un-ingested IgG-RBCs were hypotonically lysed by briefly (1–2 min) incubating the cells in 4°C water (Chow, Downey et al. 2004). Ingested IgG-RBCs were counted individually by experimenters who were blind to the genotypes and experimental conditions. Significantly fewer IgG-RBCs were internalized by ML1 KO BMMs compared with WT controls at the latter three time points (30, 60, and 90 min; Fig. 1C–E). Based on distribution histograms of the number of ingested particles per cell (Suppl.

fig. S1B), thresholds were set (4 to 10 or more particles per cell) based on the cell type and particle size to compare the phagocytic capability. Based on a threshold of 10 or more (10+) IgG-RBCs for BMMs (Fig. 1D), a significant difference in particle uptake was noted between WT and ML1 KO BMMs, with the uptake defects being more severe as time progressed (Fig. 1C–E & Suppl. fig. S1B). After 90 min, about 50% of WT, but less than 20% of ML1 KO BMMs contained 10+ internalized IgG-RBCs (Fig. 1D). The progressive inhibition of uptake caused by ML1 deficiency suggested that ML1 is necessary for the ongoing uptake of large particles, which is consistent with the reported, preferential requirement of lysosomal membrane delivery for large particle uptake (Huynh, Kay et al. 2007). To further probe this possibility, BMMs were tested for their ability to ingest different-sized IgG-opsonized polystyrene beads. Interestingly, while the internalization of 3 μm beads (a threshold of 10+ 3-μm beads set for BMMs) was similar for WT and ML1 KO BMMs, uptake of 6 μm beads (a threshold of 4+ 6-μm-beads for BMMs) was significantly reduced in ML1 KO BMMs at all time points (Fig. 1F & (Suppl. fig. S1C)). Uptake of zymosan particles (diameter = 2–3 μm) was also normal for ML1 KO BMMs (Suppl. fig. S1D). These observations are reminiscent of the particle size-dependent uptake defect seen in Syt VII$^{-/-}$ BMMs (Czibener, Sherer et al. 2006). Taken together, these results suggest that ML1 is required for efficient uptake of large particles, i.e., when the need for membranes from internal sources is high (Huynh, Kay et al. 2007).

The channel activity of ML1 regulates large particle uptake in macrophages

Next, we investigated whether increasing the expression/activity of ML1 can facilitate particle uptake in macrophages. Incubating WT BMMs with a TRPML agonist, ML-SA1 (1–10 μM), for 15 min caused more than a two-fold increase in the percentage of cells containing 10+ IgG-RBCs (Fig. 2A). In contrast, the increase was negligible for ML1 KO BMMs (Fig. 2A). Moreover, heterologous expression of ML1-GFP in ML1 KO BMMs was sufficient to restore the uptake efficiency to the same level of WT BMMs, while expression of ML1-KK-GFP, a non-conducting pore mutant of ML1 (Dong, Shen et al. 2010), had no effect (Fig. 2B). These results established a positive correlation between the channel activity of ML1 and IgG-RBC uptake.

We also examined particle uptake in RAW 264.7 macrophage cell line, as well as RAW cell lines stably expressing ML1 (ML1 overexpression or O/E) or ML1-specfic RNAi (ML1 knockdown or KD) (Thompson, Schaheen et al. 2007). ML1 expression levels in these three cell lines were confirmed using whole-endolysosome recordings (Fig. 2C) and RT-PCR analysis (Fig. 2D). Interestingly, particle uptake efficiency in these lines correlated with their respective expression levels of ML1, with an even greater correlation in the presence of ML-SA1 (Fig. 2E & Suppl. fig. S2A). The threshold of 5+ ingested IgG-RBCs was set to reflect the smaller size of RAW cells compared to BMMs. While approximately 30% of the ML1 O/E cells ingested 5+ IgG-RBCs, less than 10% of ML1 KD cells contained 5+ IgG-RBCs (Fig. 2E). Collectively, these data suggest that the efficiency of particle uptake in macrophages is positively-correlated with the expression level and channel activity of ML1.

Consistent with previous studies showing that uptake of large particles is a Ca^{2+}-dependent process in BMMs (Czibener, Sherer et al. 2006), and consistent with ML1 being a lysosomal Ca^{2+}-permeable channel (Cheng, Shen et al. 2010), pretreatment of BMMs with a membrane-permeable, fast Ca^{2+} chelator BAPTA-AM (Shen, Wang et al. 2011) inhibited particle uptake in WT macrophages but to a lower degree in ML1 KO cells (Fig. 2F). In contrast, a membrane-permeable, slow Ca^{2+} chelator EGTA-AM had little or no effect (Suppl. fig. S2B), suggesting a local source of Ca^{2+} (Shen, Wang et al. 2011).

To further investigate the role of ML1 in particle uptake, we also employed pharmacological tools to acutely inhibit the channel function of ML1. Using a Ca^{2+} imaging-based high-

throughput screening method (Shen, Wang et al. 2012), we identified three synthetic small molecule inhibitors for ML1 (Mucolipin Synthetic Inhibitor 1–3 or ML-SI1-3; see Suppl. fig. S2C & 2F). Using whole-endolysosome patch-clamp recordings, we confirmed that ML-SI1 strongly inhibited basal (Fig. 2G), ML-SA1 or PI(3,5)P_2-activated I_{ML1} (Suppl. fig. S2D). In contrast, ML-SI1 failed to inhibit PI(3,5)P_2-activated whole-endolysosome TPC2 currents (Wang, Zhang et al. 2012) (see Suppl. fig. S2E), demonstrating a relative specificity. ML-SI1 (10 μM) treatment was sufficient to reduce IgG-RBC uptake in WT BMMs to the same level as ML1 KO BMMs, without significantly affecting the uptake in ML1 KO cells (Fig. 2H). Furthermore, all three ML1 inhibitors significantly reduced the uptake of IgG-opsonized 6 μm beads (Suppl. fig. S2G). These results suggest that the channel activity of ML1 is required for large particle uptake in macrophages.

ML1 is rapidly recruited to phagocytic cups and nascent phagosomes

To investigate the mechanisms by which ML1 contributes to particle uptake, we performed timelapse confocal microscopy of live RAW cells during the particle uptake process. Strikingly, we observed that ML1-GFP was rapidly (within 1–3 min) recruited to the sites of phagosome formation during uptake of 6 μm beads (Fig. 3A and Video 1) and IgG-RBCs (Suppl. Fig S3A and Video 2). In contrast, ML1-GFP was not recruited to the sites of phagosome formation during uptake of 3 μm beads (Suppl. Fig S3B; also see Fig. 3C).

Next we compared the localization of ML1 with other endosomal and lysosomal proteins that are known to be involved in phagosome formation and maturation. Syt VII is a lysosomal Ca^{2+} sensor, but has been shown to be recruited to the nascent phagosomes upon particle binding (Czibener, Sherer et al. 2006). BMMs isolated from Syt VII KO mice exhibit a similar phenotype as ML1 KO BMMs: the defect is proportional to the particle size (Czibener, Sherer et al. 2006). Both ML1-GFP and Syt VII-mCherry were found to be co-localized at the tip of the pseudopods in doubly-transfected RAW cells (Suppl. fig. S3C). Within 2–3 mins after exposing the RAW cells to IgG-RBCs, both ML1-GFP and Syt VII-mCherry appeared on the membranes of nascent phagosomes (Fig. 3B and Video 3). ML1-GFP and Syt VII-mCherry-positive (lysosomal) tubules were then observed wrapping themselves around the newly formed phagosomes (Fig. 3B; frame 3 min 53 sec); the recruitment kinetics was similar for both proteins (Video 3).

Similar to ML1 and Syt-VII, lysosome-associated membrane protein 1 (Lamp-1) was also rapidly recruited to newly-formed large-particle-containing phagosomes in RAW macrophages BMMs (Fig. 3C). However, rapid recruitment of ML1 and Lamp1 were not seen in the presence of ML-SI1 (Suppl. Fig S3E), or for small particle uptake (Suppl. Fig S3D). The recruitment of ML1 and Lamp1 to forming phagosomes occurred prior to the recruitment of Rab5, an early phagosome maturation marker (Kitano, Nakaya et al. 2008; Guo, Hu et al. 2010), or Rab7, a late phagosome maturation marker (Henry, Hoppe et al. 2004; Guo, Hu et al. 2010) (Fig. 3C, D). Consistently, during large particle uptake, the newly formed phagosomes (5 min after particle binding) in WT BMMs, compared with ML1 KO BMMs, contained significantly more Lamp1 proteins (Suppl. fig. S3F). Phagosomes are still wrapped with polymerized actin within 5–10 min after particle binding (Suppl. fig. S3G; also see (Czibener, Sherer et al. 2006)). Collectively, these results suggest that during large particle uptake, recruitment of ML1 and other lysosomal membrane proteins occurred in the very early stages of phagosome formation, prior to Rab5-mediated early phagosome maturation. The recruitment of Lamp1 was significantly delayed in the ML1 KO BMMs, or in the presence of ML1 inhibitors (Suppl. fig. S3E), suggestive of a crucial role of ML1 in delivering lysosomal proteins and membranes to phagocytic cups.

To further separate phagosome formation from late phagosome maturation, we monitored the ML1-GFP recruitment in macrophages that were exposed to small particles. In contrast

to large particle uptake, ML1 was recruited to small particle-containing phagosomes only after 15–20 min of phagocytosis initiation (Fig. 3C, D), which was after Rab5 recruitment, but at a similar time course to Rab7 recruitment and phagosomal acidification (Suppl. fig. S3D, 3E). Hence ML1 might also play a role in late phagosome maturation.

To further confirm the presence of ML1 on the newly formed phagosomes, we developed a patch-clamp method to directly record from phagosomal membranes (Fig. 4A–B). Phagosomes were isolated from Lamp1-GFP or ML1-GFP-transfected RAW cells after exposure to IgG-RBCs or beads for 5 min. In Lamp1-GFP-transfected RAW cells, bath application of $PI(3,5)P_2$ (100 nM) or ML-SA1 (25 μM) readily activated endogenous whole-phagosome ML1-like currents (Fig. 4C). Much larger whole-phagosome ML-SA1-activated currents were seen in ML1-GFP-transfected RAW cells. In WT BMMs, whole-phagosome I_{ML1} was activated by ML-SA1, and inhibited by ML-SI1 (Fig. 4D). No significant whole-phagosome I_{ML1} was seen in ML1 KO BMMs (Fig. 4D). In contrast, $PI(3,5)P_2$-activated TPC currents (Wang, Zhang et al. 2012) was present in a subset of WT and ML1 KO BMMs (Fig. 4D). These results thus provide functional evidence that ML1 is recruited to nascent phagosomes.

Particle binding induces ML1-mediated lysosomal Ca^{2+} release and lysosomal exocytosis in macrophages

Lysosome fusion with the plasma membrane (lysosomal exocytosis) has been shown to be required for the uptake of large particles in macrophages (Czibener, Sherer et al. 2006). Fibroblasts from ML4 patients exhibit impaired lysosomal exocytosis induced by ionomycin and increased expression levels of the TFEB lysosome biogenesis transcription factor (LaPlante, Sun et al. 2006; Medina, Fraldi et al. 2011). To directly investigate the role of ML1 in lysosomal exocytosis, we acutely activated ML1 using ML-SA1 and evaluated lysosomal exocytosis by using Lamp1 surface immunostaining with the ML1 KO as the negative control. After lysosomal exocytosis, luminal lysosomal membrane proteins can be detected on the extracellular side of the plasma membrane by measuring surface expression of Lamp1 with a monoclonal antibody (1D4B) against a luminal epitope of Lamp1 (Reddy, Caler et al. 2001). After incubation with the agonist ML-SA1 for 30 min, WT, but not ML1 KO BMMs, exhibited a marked increase in Lamp1 staining (Fig. 5A & Suppl. fig. S5A, 5B). Pre-treatment with the fast Ca^{2+} chelator BAPTA-AM almost completely abolished ML-SA1-induced Lamp1 surface staining in WT BMMs (Suppl. fig. S5A). Collectively, these results suggest that the channel activity of ML1 is required for lysosomal exocytosis in macrophages in a Ca^{2+}-dependent manner.

Upon lysosomal exocytosis, lysosomal hydrolytic enzymes such as acid phosphatases (APs) are released into the extracellular medium (Reddy, Caler et al. 2001). Incubation with ML-SA1 (1 or 10 μM for 15 and 30 min) caused a significant increase in the AP release/activity in WT, but not ML1 KO BMMs (Suppl. fig. S5C, 5D). Treating cells with Ca^{2+} ionophore ionomycin induced a large AP release in ML1 KO BMMs, suggesting that the exocytosis machinery was operative (Suppl. fig. S5E). In RAW macrophage cell lines, the level of ML-SA1-induced AP release was correlated with the expression level and channel activity of ML1 (Suppl. fig. S5C). ML-SA1-induced AP release in WT BMMs was largely abolished by BAPTA-AM treatment, but not by removing extracellular Ca^{2+} (Suppl. fig. S5F).

Lysosomal membrane fusion events are presumed to be dependent on $[Ca^{2+}]_i$ increase in the close vicinity of fusion spots, though direct evidence has not been reported (Pryor, Mullock et al. 2000; Piper and Luzio 2004; Shen, Wang et al. 2011). Because ML1-GFP was co-localized with Lamp1 in the tips of pseudopods in RAW cells (Suppl. fig. S3C), we used a lysosome-targeted Genetically-Encoded Ca^{2+} Indicator, GCaMP3-ML1, to specifically measure lysosomal Ca^{2+} release in intact cells (Shen, Wang et al. 2012). Transient and

localized Ca^{2+} increases, measured with GCaMP3 fluorescence changes, were observed preferentially at the uptake sites of Syt VII-mCherry- positive lysosomes within several minutes of particle binding for both IgG-RBCs (Fig. 5B, frames 45 sec, and 3 min and 15 sec) and 6 μm beads (Suppl. fig.S5G). In contrast, little or no GCaMP3 fluorescence increase was seen in other areas of the phagocytosing macrophages within the same time course (Fig. 5B; Suppl. fig.S5H, 5I). These results suggest that particle binding induces ML1-mediated lysosomal Ca^{2+} release, locally at the sites of uptake.

To investigate the role of ML1 in lysosomal exocytosis and particle uptake, BMMs were exposed to IgG-RBCs for various lengths of time, and acid phosphatase (AP) release was measured. Compared with WT BMMs, ML1 KO cells exhibited significantly less IgG-RBC-induced AP release (Fig. 5C). Interestingly, this difference was abolished by either BAPTA-AM or inhibition of ML1 using ML-SI1 (Fig. 5C).

Next we directly investigated the insertion of ML1 onto the plasma membrane during particle uptake. Because current antibodies are inadequate for detecting endogenous ML1 proteins, we developed a whole-cell patch-clamp method to “detect” the plasma membrane insertion of ML1 during particle uptake. This electrophysiology-based “exocytosis assay” provides temporal resolution far superior to other exocytosis/secretion assays. In order to facilitate detection (by decreasing the turnover time of ML1 at the plasma membrane), we used a cell-permeable dynamin inhibitor, dynasore (Macia, Ehrlich et al. 2006), to block endocytosis that is presumed to be coupled with focal exocytosis (Lee, Mason et al. 2007; Tam, Idone et al. 2010). Large ML-SA1-induced whole-cell ML1-like currents were observed upon exposure of WT BMMs to IgG-RBCs for 10 min in the presence of dynasore (Fig. 5D, 5E). In contrast, no significant ML-SA1-induced whole-cell currents were observed in RBC-treated ML1 KO BMMs, or WT BMMs treated with dynasore alone (Fig. 5D, 5E). IgG-RBC-induced whole-cell I_{ML1} was completely inhibited by BAPTA-AM pre-treatment (Fig. 5E), suggesting that membrane insertion during phagocytosis is a Ca^{2+}-dependent process.

ML1 regulates particle ingestion via lysosomal exocytosis

To directly investigate whether the involvement of ML1 in large particle uptake is mediated by lysosomal exocytosis, we assessed particle uptake upon increasing the expression level and channel activity of ML1 while simultaneously blocking lysosomal exocytosis. Three approaches were employed to block lysosomal exocytosis. First, lysosomal exocytosis and particle uptake are inhibited by dominant-negative (DN) forms of Syt-VII (Reddy, Caler et al. 2001). We found that ML-SA1-induced large particle uptake was significantly reduced in Syt-VII-DN-transfected ML1 O/E RAW cells (Fig. 6A). Second, VAMP7 is a lysosomal SNARE protein required for lysosome-plasma membrane fusion (Braun, Fraisier et al. 2004). VAMP7 belongs to the Longin family of SNARE proteins, characterized by the presence of an auto-inhibitory domain at their N-terminus (Martinez-Arca, Rudge et al. 2003). Overexpression of the Longin domain of VAMP7 alone in macrophages is known to exert a dominant negative effect on both lysosomal exocytosis and particle uptake (Braun, Fraisier et al. 2004). ML-SA1 treatment failed to enhance particle uptake in cells transfected with Longin-GFP including ML1 O/E RAW cells (Fig. 6B) and WT BMMs (Suppl. fig. S6A), whereas overexpression of VAMP7-GFP had no inhibitory effect. Third, lysosomal exocytosis can also be reduced by treating the cells with colchicine, a known inhibitor of microtubule polymerization (Lee, Mason et al. 2007). We found that colchicine treatment significantly inhibited ML-SA1-induced large particle uptake (Fig. 6C) and lysosomal AP release (Suppl. fig. S6B) in ML1 O/E RAW cells. Taken together, these data suggest that ML1 participates in large particle uptake by regulating Ca^{2+}-dependent lysosomal exocytosis in macrophages. The residual particle uptake in ML1 KO BMMs was further inhibited by tetanus toxin (TeNT, an inhibitor of several VAMP proteins including VAMP3;

Suppl. fig. S6C), which is consistent with an additional contribution of membranes/exocytosis from recycling endosomes as reported previously (Braun, Fraisier et al. 2004).

ML1 regulates particle ingestion in a PI(3,5)P_2-dependent manner

PI(3,5)P_2 is the only known endogenous activator of ML1 (Dong, Shen et al. 2010). PI(3,5)P_2 is generated from PI(3)P by a protein complex that contains PIKfyve/Fab1, a PI-5 kinase that is localized in late endosomes and lysosomes. The activity of PIKfyve/Fab1 is dependent on the FIG4 protein in the complex (Lenk, Ferguson et al. 2011). Thus, macrophages isolated from FIG4 KO mice are predicted to have a reduced PI(3,5)P_2 level compared with WT cells (Chow, Zhang et al. 2007). FIG4 KO BMMs contained enlarged Lamp1-positive compartments (Suppl. fig. S6D), as seen in other cells types from FIG4 KO mice (Chow, Zhang et al. 2007; Lenk, Ferguson et al. 2011). Furthermore, FIG4 KO BMMs were defective in IgG-RBC uptake (Fig. 6D), and ML-SA1-or IgG-RBC-induced lysosomal AP release (Suppl. fig. S6E). Large (6 μm), but not small (3 μm) bead uptake, was also defective in WT BMMs treated with YM201636 (1 μM; Fig. 6E, 6F), a PIKfyve inhibitor (Jefferies, Cooke et al. 2008).

To directly test the possibility that an elevation of PI(3,5)P_2 is locally triggered by large particle binding, we have generated a PI(3,5)P_2-specific probe, ML1-2N-GFP, made by the fusion of GFP to the phosphoinositide-binding domain of ML1 (Li et al, manuscript in submission). The probe was mainly localized to Lamp1-positive compartments, and this localization can be altered by mutations in the probe, or by genetically or pharmacologically manipulating the PI(3,5)P_2 level, suggestive of the specificity of the probe. Strikingly, ML1-2N-GFP was rapidly recruited to the forming phagosomes (Fig. 6G) in RAW cells that were doubly transfected with ML1-2N-GFP and Syt-VII-mCherry. A transient and localized increase in ML1-2N-GFP fluorescent intensity was observed preferentially at the uptake sites of Syt-VII-mCherry-positive lysosomes within three minutes of particle binding (Fig. 6G, frame 2 min and 54 sec; Video 4). In contrast, no increase in GFP fluorescence was observed in cells transfected with ML1-7Q-2N-GFP (a PI(3,5)P_2 unbinding control probe; Li et al) (Suppl. fig. S6F). We also analyzed the kinetics of two other phosphoinositides that are known to accumulate at the site of phagocytosis. PI(3)P was detected using the 2X-FYVE-GFP probe, and PI(3,4)P_2/PI(3,4,5)P_3 was detected using the AKT-PH-GFP probe (Yeung, Ozdamar et al. 2006). The AKT-PH-GFP probe accumulated rapidly on forming phagosomes, but quickly disappeared upon closing of phagocytic cups (Suppl. fig. S6H), suggesting that the time course of PI(3,4)P_2/PI(3,4,5)P_3 transient matches phagosome formation and closure as shown previously (Yeung, Ozdamar et al. 2006). In contrast, the PI(3)P probe accumulated on the early phagosomes approximately 10 min after phagosome initiation (see Suppl. fig. S6G, H; also see ref. (Yeung, Ozdamar et al. 2006)), which was similar to Rab5 recruitment to early phagosomes. Note that PI(3)P increase occurred after Syt-VII recruitment (Suppl. fig. S6G). Because PI(3,5)P_2 accumulates at the phagocytic site in a time course similar to PI(3,4)P_2/PI(3,4,5)P_3, but prior to PI(3)P, it is very likely that PI(3,5)P_2 increase occurs during phagosome formation.

We also measured the radio-labeled phosphoinositides using high-performance liquid chromatography (HPLC) (Zolov, Bridges et al. 2012). We found that PI(3,5)P_2 levels increased significantly during the first 5 min of phagocytosis upon particle binding, which corresponds to the time necessary for phagosomes formation (Fig. 6H). These results suggest that localized PI(3,5)P_2 generation may be one of the initial steps during large particle ingestion (Fig. 6H).

ML1 deficiency results in defective clearance of senescent and apoptotic cells *in vivo*

Senescent RBCs are normally phagocytosed by macrophages in the red pulp region of the spleen, followed by the degradation of their haemoglobin and recycling of iron into the circulating blood (Bratosin, Mazurier et al. 1998). Considering that ML1 KO BMMs were defective in the uptake of large cellular particles, we investigated RBC clearance in the spleens of ML1 KO mice. In ML1 KO spleens, although Lamp1 expression was elevated (Suppl. fig. S7A, B), immuno-reactivity of the control macrophage marker CD11b was normal (Suppl. fig. S7C). ML1 KO mice exhibited enlarged spleens, but had normal kidney size, compared with WT controls (Suppl. fig. S7D, E), suggestive of compensatory changes secondary to defective clearance of senescent RBCs (Kohyama, Ise et al. 2009). Consistently, hematoxylin and eosin (H&E) staining of spleen sections revealed an accumulation of RBCs in both white and red pulps of ML1 KO but not WT spleens (Fig. 7A). In addition, ML1 KO mice had a higher level of RBCs in the blood compared with WT controls, which had a red blood cell count within the normal range (Suppl. fig. S7F).

Accumulation of RBCs in the spleen reportedly leads to a buildup of splenic iron stores (Kohyama, Ise et al. 2009). Indeed, Perl's Prussian blue staining (for ferric iron) revealed an accumulation of iron stores in the spleens of ML1 KO mice, which was largely confined to the red pulp region (Fig. 7B). Consistently, inductively-coupled plasma mass spectrometry (ICP-MS) analysis revealed that iron content was selectively increased in the ML1 KO spleens (Fig. 7C). Taken together, these results suggest that RBC clearance is defective in ML1 KO mice.

Defective phagocytosis in the brain may lead to inflammation and microglia (macrophage-like cells in the brain) activation (Venkatachalam, Long et al. 2008; Vitner, Platt et al. 2010). Consistently, Iba1, a 17-kDa EF hand protein that is specifically expressed in activated macrophage/microglia (Ferguson, Lenk et al. 2009), was up-regulated in the brain of ML1 and FIG4 KO mice (Fig. 7D, 7E). Further, massive cell death was observed in the brains of ML1 and FIG4 KO mice (Fig. 7F).

Discussion

Using pharmacological, genetic, and biochemical approaches, we demonstrate that the channel activity of ML1 is necessary for efficient uptake of large particles in macrophages. Live imaging and electrophysiological recordings reveal that ML1 is rapidly activated and recruited to the membrane extensions surrounding the particles in the process of phagocytic internalization. Our results are compatible with the following working model: large particle binding to macrophages triggers $PI(3,5)P_2$ elevation, which induces ML1-mediated lysosomal Ca^{2+} release and lysosomal exocytosis at the sites of uptake (see Fig. 6I).

The activation of IgG Fc receptors during phagocytosis has been known to induce a transient increase in $[Ca^{2+}]_i$ in neutrophils (Myers and Swanson 2002; Nunes and Demaurex 2010). This was not seen in macrophages (Nunes and Demaurex 2010). Using our recently-established lysosome-specific Ca^{2+} imaging method with lysosome-targeted genetically-encoded Ca^{2+} sensor GCaMP3, which is more sensitive in detecting lysosomal Ca^{2+} release than conventional methods, we indeed found that particle binding to macrophages also induces Ca^{2+} increase, but exclusively at the site of the particle uptake. Furthermore, the present study has extended the earlier observations by demonstrating that transient Ca^{2+} release from the lysosomes through ML1 is responsible for triggering lysosomal exocytosis during the uptake of large particles. Additionally, acidic granules in neutrophils (equivalent to lysosomes in macrophages) have been shown to redistribute toward the site of particle uptake, suggesting a source of membrane (Stendahl, Krause et al. 1994; Tapper, Furuya et al. 2002). Using time-lapse live imaging, we have demonstrated that lysosomes and their

resident proteins are also redistributed toward the site of uptake in macrophages. Thus, lysosomes serve uniquely as sources not only for membranes, but also for Ca^{2+} that is required for Syt-VII activation/recruitment.

What differentiates the uptake of large *vs.* small particles is not clear. A small increase in the diameter of particle may result in a much larger demand for membranes, receptors, signaling molecules, and cytoskeleton machinery. It is known that the uptake of large (> 4.5 μm) IgG-coated particles depends on phosphatidylinositol 3-kinase (PI3K) activity, whereas the uptake of smaller (< 3 μm) particles does not require PI3K activity (Cox, Tseng et al. 1999). For example, wortmannin and LY294002, two non-specific type I & II PI3K inhibitors, preferentially inhibit the uptake of large particles (Cox, Tseng et al. 1999; Hoppe and Swanson 2004). While type I PI3K has been linked to an effect on cytoskeleton rearrangement during large particle uptake (Cox, Tseng et al. 1999; Hoppe and Swanson 2004), type II PI3K could contribute to large particle uptake via the production of PI(3)P, the precursor of $PI(3,5)P_2$, which in turn is the endogenous activator of ML1 (Shen, Wang et al. 2012). BMMs with reduced $PI(3,5)P_2$ levels also exhibit the size-dependent uptake phenotype. It is possible that $PI(3,5)P_2$ production, as detected using our genetically-encoded $PI(3,5)P_2$ sensor, may be the key signaling event that leads to ML1 activation and subsequent lysosomal exocytosis (see Fig. 6H, 6G).

We have shown that during large particle uptake, ML1, Syt-VII, and Lamp1 are rapidly delivered to forming phagosomes. The early recruitment of Syt-VII and Lamp1 within 5 min of phagocytosis initiation is impaired when the activity of ML1 is inhibited, and is not seen for small particle uptake. In late phagosome maturation, lysosomal membrane proteins are also expected to appear on the phagosomal membranes through phagosome-lysosome fusion (Flannagan, Jaumouille et al. 2012). Indeed, in contrast to large particle uptake, ML1-GFP was recruited only after 20 min of phagocytosis initiation in small particle uptake. Therefore, lysosomes play dual roles sequentially in (nascent) phagosome formation and (late) phagosome formation, and are delivered to the phagosomes at two different stages. First, for large particles, lysosomes fuse with the plasma membrane at the phagocytic cup, which provides the membranes necessary for phagosome formation. As a result, lysosomal membrane proteins such as ML1 and Lamp1 are delivered to the newly formed phagosomes, prior to or during phagocyt ic cup closing. This is a path via lysosomal exocytosis that occurs early during phagosome formation. Second, for both large and small particles, lysosomes are also delivered to the late phagosomes through late phagosome maturation (phagosome-lysosome fusion), which is required for the degradation of phagocytic materials. This second stage is accompanied by Rab7 recruitment and phagosomal acidification, as well as further recruitment of lysosomal membrane proteins including ML1 and Lamp1. This is a path that occurs late during phagosome-lysosome fusion. As discussed in previous studies (Czibener, Sherer et al. 2006), the early recruitment of lysosomal membrane proteins may serve as a rather early preparation for phagosome maturation, especially for large particle uptake, but is not completely essential for phagosome maturation.

Our results in the present study are consistent with previous reports showing that the clearance of late apoptotic neurons is impaired in the *Drosophila* TRPML mutant (Venkatachalam, Long et al. 2008), suggesting that TRPML channels play a role in eliminating pathogenic extracellular particles. Extracellular accumulation of large particles such as apoptotic cells may cause brain inflammation and microglia activation, which are common features in most neurodegenerative Lysosome Storage Diseases (LSDs) (Vitner, Platt et al. 2010). It is possible that defective phagocytosis of large particle is a general pathogenic factor for many LSDs, with ML1 channel deregulation in phagocytes being a primary cause.

Experimental Procedures

Phagocytosis assay

Sheep RBCs (Lampire Biological Laboratories) were washed twice with PBS and then fixed with 4% paraformaldehyde (PFA) overnight at 4°C in an end-over-end rotator. Free aldehyde groups were quenched by re-suspension in PBS containing 100 mM glycine for 30 min at 4°C; RBCs were opsonized with rabbit IgG antibody (Equitech-Bio, Inc) at 37°C for 1h. Phagocytosis was initiated by adding IgG-RBCs onto adherent BMMs at a ratio of 50:1 (RBC: BMM). To synchronize binding and internalization, IgG-RBCs were centrifuged at 300 rpm for 3 min together with adherent BMMs. BMMs were placed at 37°C and 5% CO_2 for various time points (15–90 min). Non-ingested IgG-RBCs were lysed by incubating the cells with water (1 ml) for 2–3 min at 4°C (Chow, Downey et al. 2004). RBC-containing BMMs were fixed in 2% PFA and stained with goat-anti rabbit IgG AlexaFluor488 (1:500 dilution, Invitrogen). Approximately 150–200 BMMs were typically analyzed for each experiment. Ingested RBCs were counted by experimenters who were blinded to the genotype and treatment.

Whole-phagosome electrophysiology

RAW macrophages and BMMs were transfected with Lamp1-GFP or ML1-GFP using the Neon electroporation system (Invitrogen, MPK 5000). IgG-RBCs were first incubated with macrophages at 4°C for 20 min to synchronize the binding of IgG-RBCs to cells. After several gentle washes, cells were placed at 37°C and 5% CO_2 for 5 min to initiate the phagocytosis, and then transferred to room temperature to slow down the phagocytosis (Holevinsky and Nelson 1998). Within 5 min of phagocytosis initiation, the phagosomes formed at this stage were not fused with lysosomes (Vieira, O., Botelho, R., Grinstein, S., 2002), and were considered as newly-formed or nascent phagosomes. Because the majority of RBC-containing phagosomes (~5 μm, roughly as the size of RBCs) were also Lamp1-GFP or ML1-GFP-positive (see Fig. 4), the GFP-positive vesicles (~ 5 μm) were identified as nascent phagosomes. Patch-clamp recordings were performed on the isolated newly-formed phagosomes (see Fig. 4). To isolate phagosomes, a patch pipette was used to open the cell by slicing the cell membrane. Then phagosomes were released into the dish and recognized by GFP fluorescence. The bath (cytoplasmic) solution contained 140 mM K-gluconate, 4 mM NaCl, 1 mM EGTA, 2 mM $MgCl_2$, 0.39 mM $CaCl_2$, and 10 mM HEPES (pH adjusted with KOH to 7.2; free [Ca^{2+}] ~100 nM). The pipette (luminal) solution contained 145 mM NaCl, 5 mM KCl, 2 mM CaCl2, 1 mM $MgCl_2$, 10 mM HEPES, 10 mM MES, and 10 mM glucose (pH 6.5, adjusted with NaOH). Data were collected and analyzed as described in Extended Experimental Procedures in the Supplementary Information.

GCaMP3 and Fura-2 Ca^{2+} imaging

Ca^{2+} imaging was performed as described in Extended Experimental Procedures in the Supplementary Information.

Lysosomal enzyme release/activity

Lysosomal enzyme release was measured as described in Extended Experimental Procedures in the Supplementary Information.

HPLC measurement of phosphoinositide levels

Phosphoinositides are radio-labeled and measured as described in Extended Experimental Procedures in the Supplementary Information.

Data analysis

Data are presented as the mean ± standard error of the mean (SEM). Statistical comparisons were made using analysis of variance (ANOVA). A P value < 0.05 was considered statistically significant.

Supplementary Material

Refer to Web version on PubMed Central for supplementary material.

Acknowledgments

This work was supported by NIH grants (NS062792, MH096595, and AR060837 to H.X, GM24872 to M. Meisler, and NS064015 to L.S.W). We are grateful to Dr. Loren Looger for the GCaMP3 construct, Drs. Norma Andrews and Thomas Sudhof for Syt-VII construct, Florence Niedergang and Robert Edwards for VAMP7 constructs, Ed Stuenkel for the TeNT construct, Johnny Fares for ML1-overexpressing or knockdown RAW macrophages, Gregg Sobocinski for assistance in confocal imaging, and Richard Hume and Miriam Meisler for comments on an earlier version of the manuscript. We appreciate the encouragement and helpful comments from other members of the Xu laboratory.

References

Aderem A, Underhill DM. Mechanisms of phagocytosis in macrophages. Annu Rev Immunol. 1999; 17:593–623. [PubMed: 10358769]

Andrews NW. Regulated secretion of conventional lysosomes. Trends Cell Biol. 2000; 10(8):316–321. [PubMed: 10884683]

Bajno L, Peng XR, et al. Focal exocytosis of VAMP3-containing vesicles at sites of phagosome formation. J Cell Biol. 2000; 149(3):697–706. [PubMed: 10791982]

Bratosin D, Mazurier J, et al. Cellular and molecular mechanisms of senescent erythrocyte phagocytosis by macrophages. A review. Biochimie. 1998; 80(2):173–195. [PubMed: 9587675]

Braun V, Fraisier V, et al. TI-VAMP/VAMP7 is required for optimal phagocytosis of opsonised particles in macrophages. EMBO J. 2004; 23(21):4166–4176. [PubMed: 15470500]

Braun V, Niedergang F. Linking exocytosis and endocytosis during phagocytosis. Biol Cell. 2006; 98(3):195–201. [PubMed: 16480341]

Cheng X, Shen D, et al. Mucolipins: Intracellular TRPML1-3 channels. FEBS Lett. 2010; 584(10): 2013–2021. [PubMed: 20074572]

Chow CW, Downey GP, et al. Measurements of phagocytosis and phagosomal maturation. Curr Protoc Cell Biol. 2004; Chapter 15(Unit 15):17.

Chow CY, Zhang Y, et al. Mutation of FIG4 causes neurodegeneration in the pale tremor mouse and patients with CMT4J. Nature. 2007; 448(7149):68–72. [PubMed: 17572665]

Cox D, Tseng CC, et al. A requirement for phosphatidylinositol 3-kinase in pseudopod extension. J Biol Chem. 1999; 274(3):1240–1247. [PubMed: 9880492]

Czibener C, Sherer NM, et al. Ca2+ and synaptotagmin VII-dependent delivery of lysosomal membrane to nascent phagosomes. J Cell Biol. 2006; 174(7):997–1007. [PubMed: 16982801]

Dong XP, Cheng X, et al. The type IV mucolipidosis-associated protein TRPML1 is an endolysosomal iron release channel. Nature. 2008; 455(7215):992–996. [PubMed: 18794901]

Dong XP, Shen D, et al. PI(3,5)P(2) controls membrane trafficking by direct activation of mucolipin Ca(2+) release channels in the endolysosome. Nat Commun. 2010; 1:38. [PubMed: 20802798]

Ferguson CJ, Lenk GM, et al. Defective autophagy in neurons and astrocytes from mice deficient in PI(3,5)P2. Hum Mol Genet. 2009; 18(24):4868–4878. [PubMed: 19793721]

Flannagan RS, Jaumouille V, et al. The cell biology of phagocytosis. Annu Rev Pathol. 2012; 7:61–98. [PubMed: 21910624]

Guo P, Hu T, et al. Sequential action of Caenorhabditis elegans Rab GTPases regulates phagolysosome formation during apoptotic cell degradation. Proc Natl Acad Sci U S A. 2010; 107(42):18016–18021. [PubMed: 20921409]

Hackam DJ, Rotstein OD, et al. v-SNARE-dependent secretion is required for phagocytosis. Proc Natl Acad Sci U S A. 1998; 95(20):11691–11696. [PubMed: 9751727]

Henry RM, Hoppe AD, et al. The uniformity of phagosome maturation in macrophages. J Cell Biol. 2004; 164(2):185–194. [PubMed: 14718518]

Holevinsky KO, Nelson DJ. Membrane capacitance changes associated with particle uptake during phagocytosis in macrophages. Biophys J. 1998; 75(5):2577–2586. [PubMed: 9788954]

Hoppe AD, Swanson JA. Cdc42, Rac1, and Rac2 display distinct patterns of activation during phagocytosis. Mol Biol Cell. 2004; 15(8):3509–3519. [PubMed: 15169870]

Huynh KK, Kay JG, et al. Fusion, fission, and secretion during phagocytosis. Physiology (Bethesda). 2007; 22:366–372. [PubMed: 18073409]

Jefferies HB, Cooke FT, et al. A selective PIKfyve inhibitor blocks PtdIns(3,5)P(2) production and disrupts endomembrane transport and retroviral budding. EMBO Rep. 2008; 9(2):164–170. [PubMed: 18188180]

Kitano M, Nakaya M, et al. Imaging of Rab5 activity identifies essential regulators for phagosome maturation. Nature. 2008; 453(7192):241–245. [PubMed: 18385674]

Kohyama M, Ise W, et al. Role for Spi-C in the development of red pulp macrophages and splenic iron homeostasis. Nature. 2009; 457(7227):318–321. [PubMed: 19037245]

LaPlante JM, Sun M, et al. Lysosomal exocytosis is impaired in mucolipidosis type IV. Mol Genet Metab. 2006; 89(4):339–348. [PubMed: 16914343]

Lee WL, Mason D, et al. Quantitative analysis of membrane remodeling at the phagocytic cup. Mol Biol Cell. 2007; 18(8):2883–2892. [PubMed: 17507658]

Lenk GM, Ferguson CJ, et al. Pathogenic mechanism of the FIG4 mutation responsible for Charcot-Marie-Tooth disease CMT4J. PLoS Genet. 2011; 7(6):e1002104. [PubMed: 21655088]

Macia E, Ehrlich M, et al. Dynasore, a cell-permeable inhibitor of dynamin. Dev Cell. 2006; 10(6): 839–850. [PubMed: 16740485]

Martinez-Arca S, Rudge R, et al. A dual mechanism controlling the localization and function of exocytic v-SNAREs. Proc Natl Acad Sci U S A. 2003; 100(15):9011–9016. [PubMed: 12853575]

Medina DL, Fraldi A, et al. Transcriptional activation of lysosomal exocytosis promotes cellular clearance. Dev Cell. 2011; 21(3):421–430. [PubMed: 21889421]

Myers JT, Swanson JA. Calcium spikes in activated macrophages during Fcgamma receptor-mediated phagocytosis. J Leukoc Biol. 2002; 72(4):677–684. [PubMed: 12377936]

Niedergang F, Chavrier P. Signaling and membrane dynamics during phagocytosis: many roads lead to the phagos(R)ome. Curr Opin Cell Biol. 2004; 16(4):422–428. [PubMed: 15261675]

Nunes P, Demaurex N. The role of calcium signaling in phagocytosis. J Leukoc Biol. 2010; 88(1):57–68. [PubMed: 20400677]

Piper RC, Luzio JP. CUPpling calcium to lysosomal biogenesis. Trends Cell Biol. 2004; 14(9):471–473. [PubMed: 15350973]

Pryor PR, Mullock BM, et al. The role of intraorganellar Ca(2+) in late endosome-lysosome heterotypic fusion and in the reformation of lysosomes from hybrid organelles. J Cell Biol. 2000; 149(5):1053–1062. [PubMed: 10831609]

Reddy A, Caler EV, et al. Plasma membrane repair is mediated by Ca(2+)-regulated exocytosis of lysosomes. Cell. 2001; 106(2):157–169. [PubMed: 11511344]

Shen D, Wang X, et al. Lipid storage disorders block lysosomal trafficking by inhibiting a TRP channel and lysosomal calcium release. Nat Commun. 2012; 3:731. [PubMed: 22415822]

Shen D, Wang X, et al. Pairing phosphoinositides with calcium ions in endolysosomal dynamics: phosphoinositides control the direction and specificity of membrane trafficking by regulating the activity of calcium channels in the endolysosomes. Bioessays. 2011; 33(6):448–457. [PubMed: 21538413]

Stendahl O, Krause KH, et al. Redistribution of intracellular Ca2+ stores during phagocytosis in human neutrophils. Science. 1994; 265(5177):1439–1441. [PubMed: 8073285]

Sun M, Goldin E, et al. Mucolipidosis type IV is caused by mutations in a gene encoding a novel transient receptor potential channel. Hum Mol Genet. 2000; 9(17):2471–2478. [PubMed: 11030752]

Swanson J, Bushnell A, et al. Tubular lysosome morphology and distribution within macrophages depend on the integrity of cytoplasmic microtubules. Proc Natl Acad Sci U S A. 1987; 84(7): 1921–1925. [PubMed: 3550801]

Tam C, Idone V, et al. Exocytosis of acid sphingomyelinase by wounded cells promotes endocytosis and plasma membrane repair. J Cell Biol. 2010; 189(6):1027–1038. [PubMed: 20530211]

Tapper H, Furuya W, et al. Localized exocytosis of primary (lysosomal) granules during phagocytosis: role of Ca2+-dependent tyrosine phosphorylation and microtubules. J Immunol. 2002; 168(10): 5287–5296. [PubMed: 11994486]

Tapper H, Sundler R. Glucan receptor and zymosan-induced lysosomal enzyme secretion in macrophages. Biochem J. 1995; 306(Pt 3):829–835. [PubMed: 7702580]

Theler JM, Lew DP, et al. Intracellular pattern of cytosolic Ca2+ changes during adhesion and multiple phagocytosis in human neutrophils. Dynamics of intracellular Ca2+ stores. Blood. 1995; 85(8):2194–2201. [PubMed: 7718891]

Thompson EG, Schaheen L, et al. Lysosomal trafficking functions of mucolipin-1 in murine macrophages. BMC Cell Biol. 2007; 8:54. [PubMed: 18154673]

Touret N, Paroutis P, et al. Quantitative and dynamic assessment of the contribution of the ER to phagosome formation. Cell. 2005; 123(1):157–170. [PubMed: 16213220]

Venkatachalam K, Long AA, et al. Motor deficit in a Drosophila model of mucolipidosis type IV due to defective clearance of apoptotic cells. Cell. 2008; 135(5):838–851. [PubMed: 19041749]

Venugopal B, Browning MF, et al. Neurologic, gastric, and opthalmologic pathologies in a murine model of mucolipidosis type IV. Am J Hum Genet. 2007; 81(5):1070–1083. [PubMed: 17924347]

Vieira OV, Botelho RJ, et al. Phagosome maturation: aging gracefully. Biochem J. 2002; 366(Pt 3): 689–704. [PubMed: 12061891]

Vitner EB, Platt FM, et al. Common and uncommon pathogenic cascades in lysosomal storage diseases. J Biol Chem. 2010; 285(27):20423–20427. [PubMed: 20430897]

Wang X, Zhang X, et al. TPC Proteins Are Phosphoinositide- Activated Sodium-Selective Ion Channels in Endosomes and Lysosomes. Cell. 2012; 151(2):372–383. [PubMed: 23063126]

Yeung T, Ozdamar B, et al. Lipid metabolism and dynamics during phagocytosis. Curr Opin Cell Biol. 2006; 18(4):429–437. [PubMed: 16781133]

Zolov SN, Bridges D, et al. In vivo, Pikfyve generates PI(3,5)P2, which serves as both a signaling lipid and the major precursor for PI5P. Proc Natl Acad Sci U S A. 2012; 109(43):17472–17477. [PubMed: 23047693]

Highlights

- • Phagocytic uptake of apoptotic bodies is defective in TRPML1 knockout macrophages
- • Large particle binding induces lysosomal PI(3,5)P2 elevation in macrophages.
- • Particle binding activates TRPML1, lysosomal Ca^{2+} release, and focal exocytosis
- • Focal exocytosis provides intracellular membranes for phagosome biogenesis.

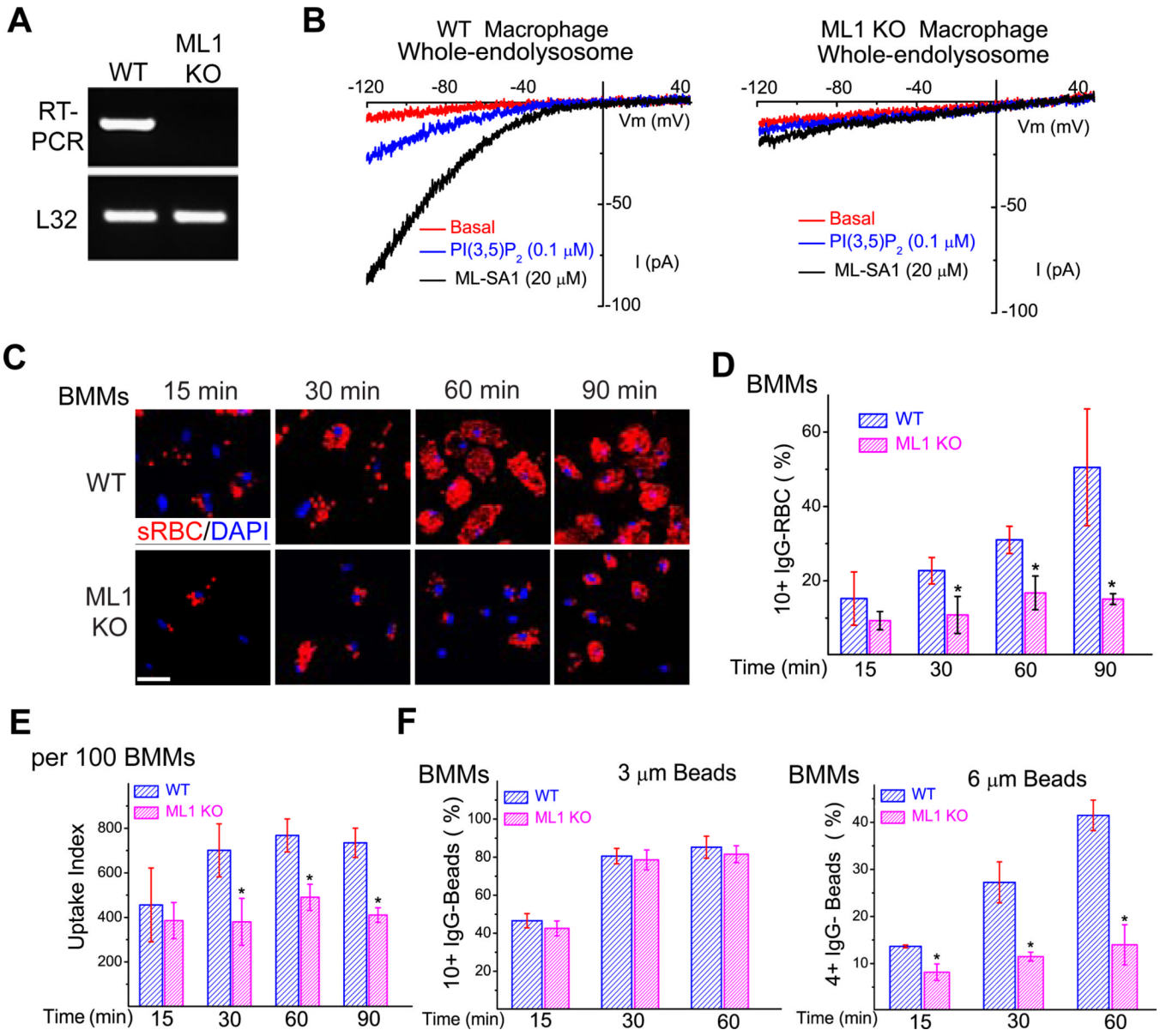

Figure 1. TRPML1 is necessary for optimal phagocytosis of large particles in bone-marrow macrophages

(A) RT-PCR analysis of wild type (WT) and TRPML1 KO (ML1 KO) bone-marrow derived macrophages (BMMs) using a primer pair targeting the deleted region (exons 3, 4, and 5) of the *TRPML1* gene (Venugopal, Browning et al. 2007). The housekeeping gene L32 served as a loading control. **(B)** ML-SA1 robustly activated endogenous whole-endolysosome ML1-like currents in WT, but not ML1 KO BMMs. **(C)** WT and ML1 KO BMMs were exposed to IgG-opsonized red blood cells (IgG-RBCs; red colored) at a ratio of 50 RBCs/BMM for time periods indicated (15, 30, 60, and 90 min). Non-ingested IgG-RBCs were lysed by briefly (1–2 min) incubating the cells in water at 4°C. Samples were then fixed and processed for confocal microscopy. **(D)** Average particle ingestion for WT and ML1 KO BMMs. Ingested IgG-RBCs were quantified for 150–200 BMMs per experiment, by experimenters who were blind to the genotype. **(E)** ML1 KO BMMs had a lower uptake index compared with WT BMMs. Uptake index was calculated based on the

total number of RBCs ingested for 100 BMMs. **(F)** Particle-size-dependent phagocytosis defect of ML1 KO BMMs. BMMs were exposed to 3 or 6 μm IgG-coated polystyrene beads for indicated periods of time. Samples were washed extensively and briefly trypsinized to dissociate non-ingested beads attached to the cell surface or cover slips. The number of ingested particles was determined as described in (**D**). For all panels, unless otherwise indicated, the data represent the mean ± the standard error of the mean (SEM) from at least three independent experiments. See also Figure S1.

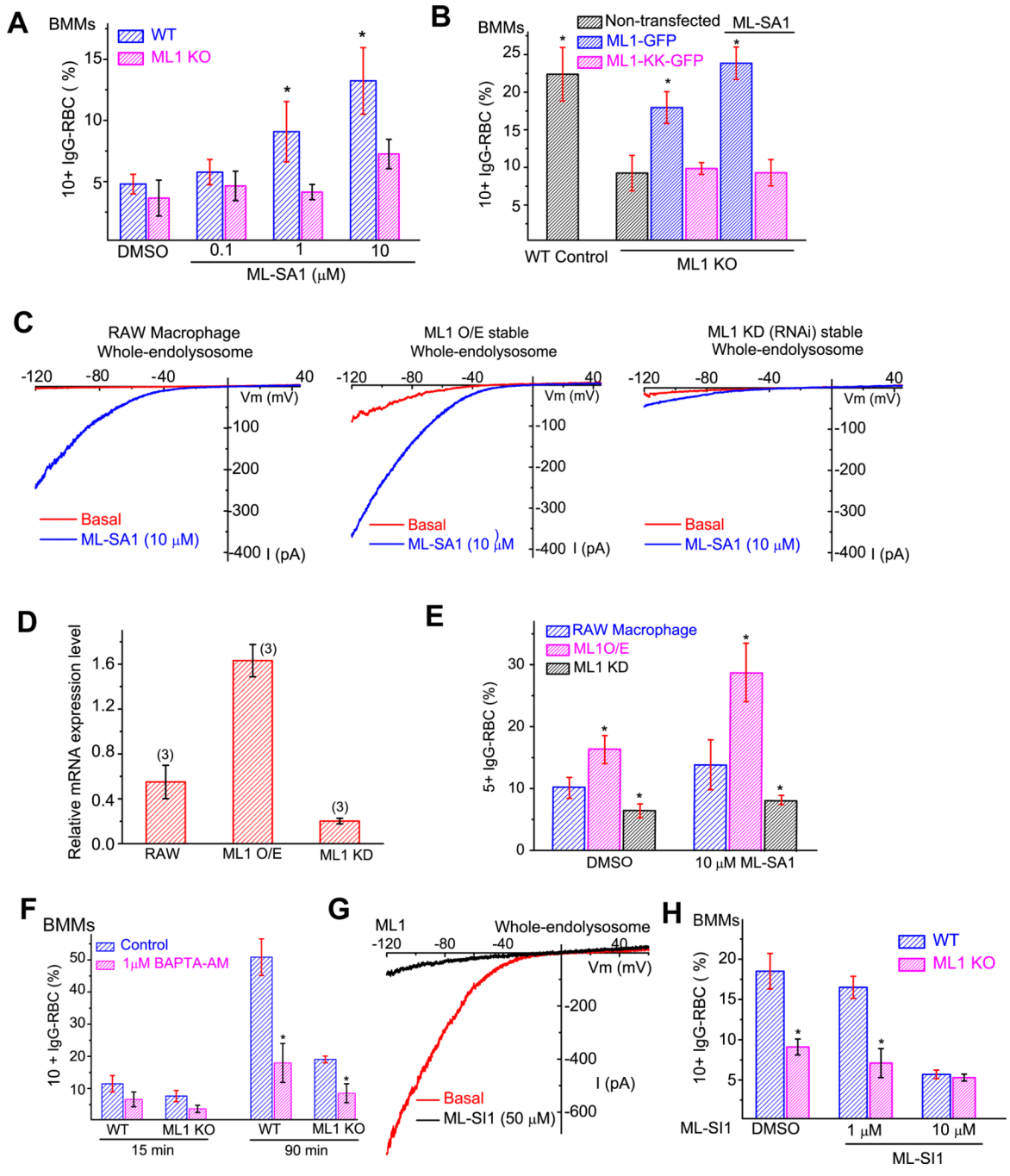

Figure 2. The expression level and channel activity of ML1 regulate particle ingestion in macrophages

(A) Micromolar concentrations of ML-SA1 (0.1, 1, and 10 μM; pre-incubation for 15 min) increased particle uptake in WT, but not ML1 KO BMMs. BMMs were exposed to IgG-RBCs in the presence of ML-SA1 for 15 min. **(B)** Transfection of ML1-GFP, but not ML1-KK-GFP (non-conducting pore mutation (Dong, Shen et al. 2010), rescued the uptake defect in ML1 KO BMMs. BMMs were exposed to IgG-RBCs for 30 min in the presence or absence of the small molecule TRPML agonist, ML-SA1 (10 μM). **(C)** ML-SA1-activated whole-endolysosome TRPML-like currents in RAW 264.7 macrophage cell lines, RAW cells stably-expressing ML1-GFP (ML1 overexpression or O/E), and RAW cells stably-

expressing ML1-specific RNAi (ML1 knockdown or KD) (Thompson, Schaheen et al. 2007). **(D)** Real-time RT-PCR analysis of ML1 RNA expression level (relative to L32) in RAW macrophages (N=3 batches of independent experiments for each cell type). **(E)** Particle uptake in RAW 264.7, ML1 O/E, and ML1 KD RAW macrophages. **(F)** Particle uptake was sensitive to intracellular Ca^{2+}. BMMs were pre-incubated with the membrane-permeable fast Ca^{2+} chelator BAPTA-AM (1 μM; 15 min) prior to IgG-RBC exposure. **(G)** ML-SI1 inhibited large basal whole-endolysosome I_{ML1} that was seen in a subset of ML1-expressing Cos1 cells. **(H)** ML-SI1 (10 μM; pre-incubation for 15 min) inhibited particle ingestion in WT BMMs to a similar level of that in ML1 KO BMMs. BMMs were exposed to IgG-RBCs in the presence of ML-SI1 for 30 min. For all panels, unless otherwise indicated, the data represent the mean ± SEM from at least three independent experiments; 150–200 BMMs were analyzed for each experiment. See also Figure S2.

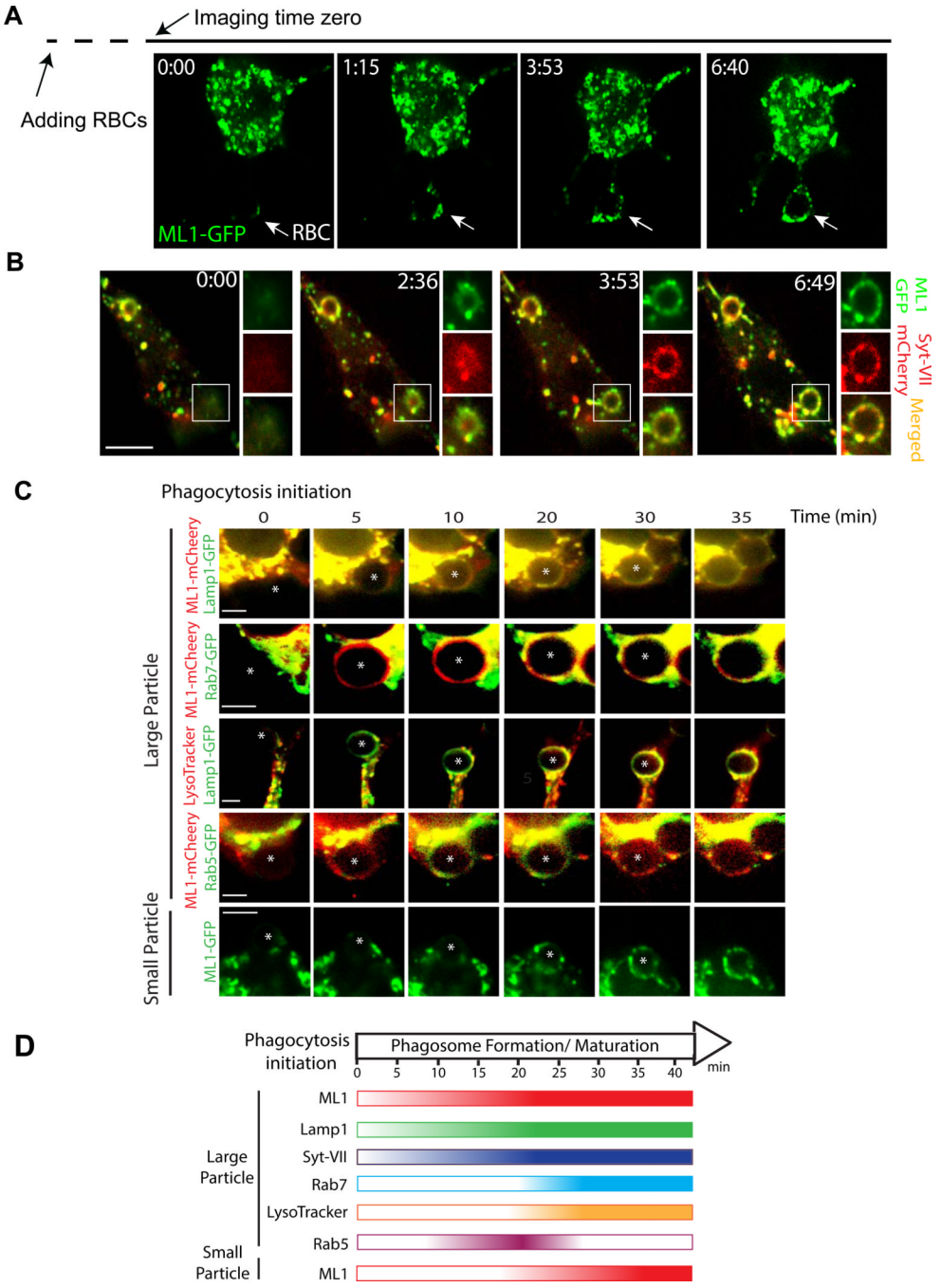

Figure 3. Particle binding to macrophages rapidly recruits ML1-GFP to the phagocytic cups and nascent phagosomes

(A) Rapid recruitment of ML1-GFP to the sites of particle ingestion (white arrow) and to expanding membrane extensions. Selected frames from time-lapse confocal microscopy of a ML1-GFP transfected RAW 264.7 macrophage that was exposed to 6 μm IgG-coated polystyrene beads. Approximately one min after the attachment of beads to the cell surface, ML1-GFP was recruited to the membrane extension surrounding the particle (Frame 1 min 15 sec; Video 1). Note that phagocytosis may have been initiated before the imaging time zero due to a technical difficulty in identifying phagocytosing macrophages and capturing phagocytosing events, which typically took 5–10 min after RBCs were added to the

recording chamber. Scale bar = 5 μm. **(B**) ML1-GFP and Syt VII-mCherry were simultaneously recruited to nascent phagosomes. Selected frames from time-lapse confocal microscopy (Video 3) showed a RAW cell doubly-transfected with ML1-GFP and Syt VII-mCherry that was exposed to IgG-RBCs. White box indicates the site of particle ingestion; both ML1-GFP and Syt VII-mCherry were concurrently recruited to the site of phagosome formation. Scale bar = 10 μm. **(C)** The recruitment kinetics of different endolysosomal markers to the particle-containing phagosomes. RAW macrophage cells were transfected with various molecular endosomal and lysosomal markers. Upon particle binding, the recruitment of these markers to phagosomes was monitored using live-cell imaging over the course of 40 min. For large particles, ML1-mCherry and Lamp1-GFP were recruited to the forming phagosomes within 5 min after phagocytosis initiation; Rab7-GFP and LysoTracker were observed in the phagosomes about 20 min after phagocytosis initiation; Rab5-GFP appeared on the phagosomes 10 min after phagocytosis initiation, and then disappeared 10 – 15 min later. For small particles (bottom row), ML1-GFP was recruited to the small particle-containing phagosomes 15–20 min after phagocytosis initiation. The center of the particle is indicated with an *. Scale bars = 5 μm. **(D)** Summary of recruitment kinetics of various endolysosomal markers to phagosomes. See also Figure S3.

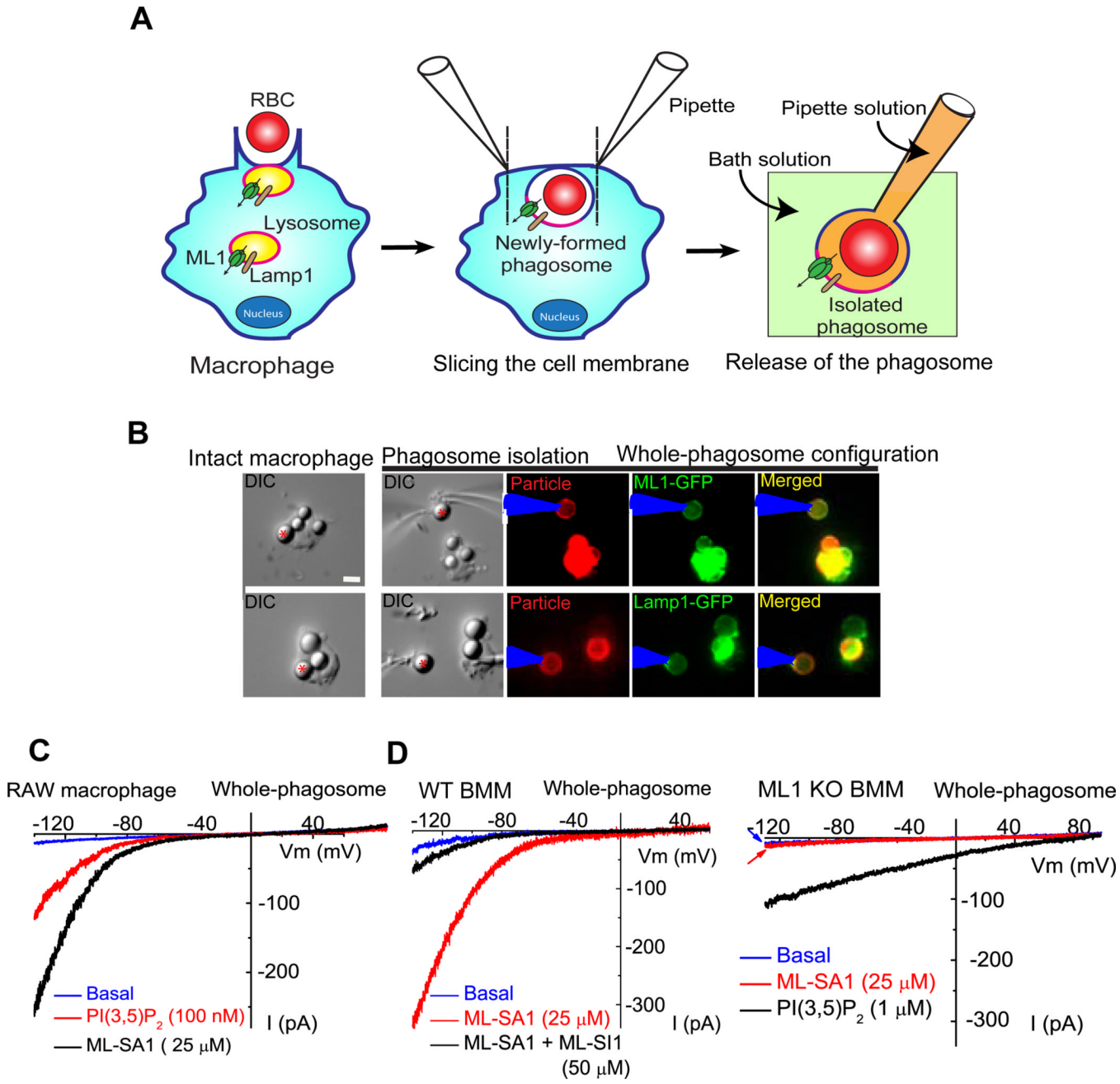

Figure 4. Whole-phagosome recording of ML1 channels in the isolated nascent phagosomes

(A) Cartoon illustrations of whole-phagosome recording procedures. Upon RBC uptake (left panel), patch electrodes are used to slice open the phagocytosing macrophage within 5 min of particle binding and ingestion. After RBC-containing phagosomes are isolated, a patch pipette is used to achieve the whole-phagosome configuration. **(B)** An illustration of whole-phagosome configuration. Cells were transfected with Lamp-1-GFP or ML1-GFP and then exposed to IgG-coated beads on ice for 20 min; after phagocytosis was induced by transferring the cells to 37°C for 5 min, the newly formed phagosomes were isolated for electrophysiology. **(C)** ML-SA1- or $PI(3,5)P_2$-activated endogenous whole-phagosome TRPML-like currents in RAW 246.7 cells. **(D)** Whole-phagosome I_{ML1} in WT, but not ML1 KO BMMs. ML-SA1 (25 μM) - activated I_{ML1} was inhibited by ML-SI1 (50 μM) in WT

phagosomes (left panel). No ML-SA1- activated I_{ML1} was seen in ML1 KO phagosomes, in which PI(3,5)P_2 (1 μM) robustly activated I_{TPC}.

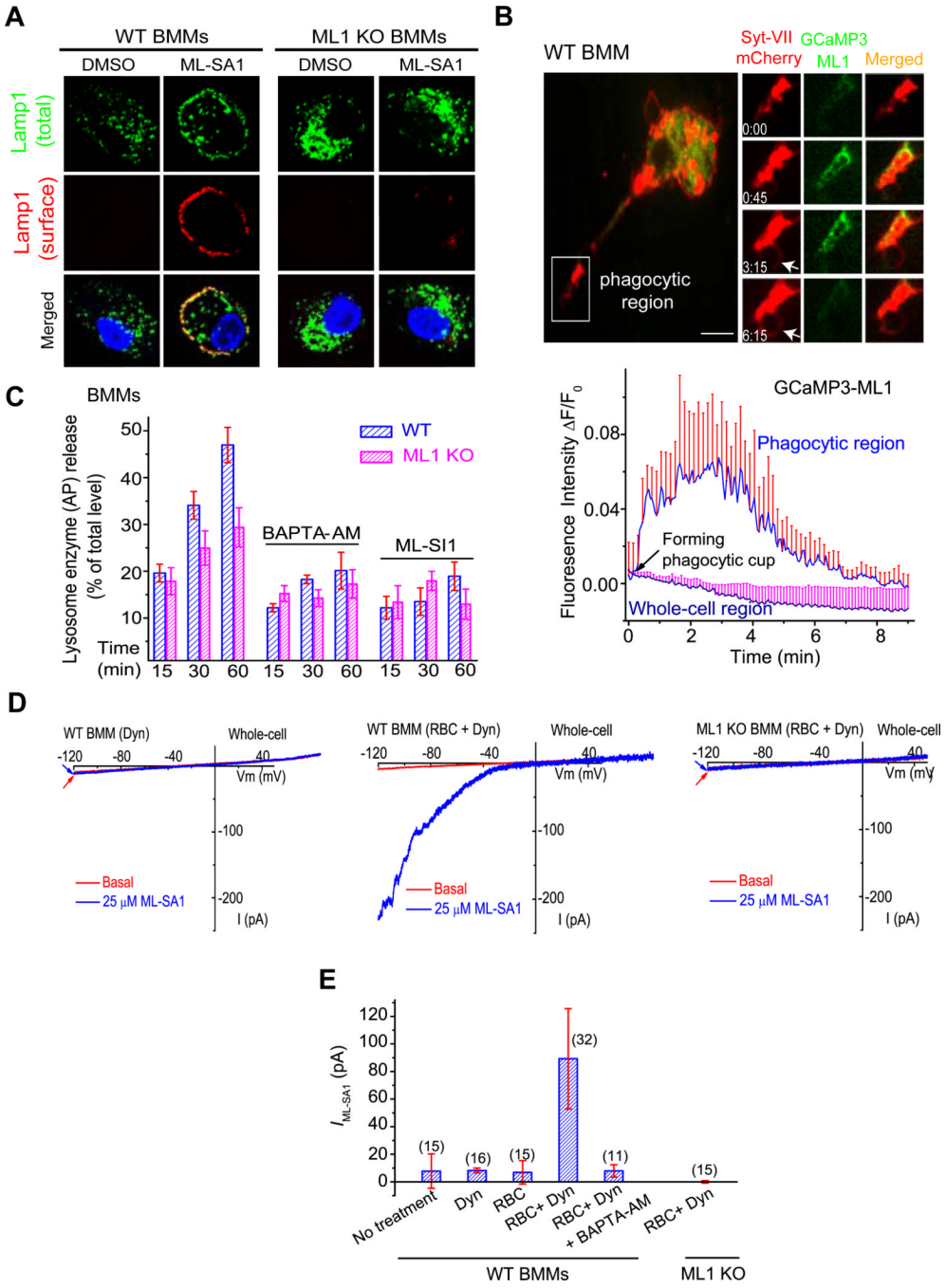

Figure 5. Particle binding induces ML1-dependent lysosomal Ca^{2+} release and lysosomal exocytosis in macrophages

(**A**) ML-SA1 (10 μM for 30 min) treatment resulted in localization of Lamp1 (red) on the plasma membrane in non-permeabilized WT, but not ML1 KO BMMs. Lamp1 surface expression was detected using an antibody recognizing a luminal epitope (1DB4). After the cells were permeabilized, total (cell surface + intracellular; green) Lamp1 proteins were detected by using the same antibody. Scale bar = 5 μm. (**B**) IgG-RBC binding triggered a localized Ca^{2+} increase at the site of uptake, shown with selected image frames of a RAW cell doubly-transfected with GCaMP3-ML1 and Syt VII-mCherry. Upon IgG-RBC binding, GCaMP3-ML1 fluorescence increased rapidly (frame 0 min 45 sec) near the site of uptake

and around the Syt VII-mCherry-positive compartments in the membrane extension, and then decreased after phagosome formation (frame 6 min 15 sec). Lower panel shows the time-dependent changes of GCaMP3-ML1 fluorescence upon particle binding, at the site of uptake (phagocytic region) and in the cell body (whole-cell region). White arrow indicates the phagocytic cup. Scale bar = 10 μm. (**C**) RBC-ingestion-induced lysosomal acid phosphatase (AP) release in WT BMMs was reduced by treatment of BAPTA-AM (500 nM, pre-incubation for 15 min) or ML-SI1 (10 μM, pre-incubation for 10 min). (**D**) Whole-cell ML1-like currents in WT BMMs that were exposed to IgG-RBCs for 10 min. Dynasore (Dyn, 100 μM) was used to block Dynamin-dependent endocytosis to facilitate the detection of whole-cell I_{ML1}. No significant whole-cell I_{ML1} was detected in ML1 KO BMMs (IgG-RBCs for 10 min). (**E**) Summary of whole-cell I_{ML1} under different experimental conditions. For all panels, unless otherwise indicated, the data represent the mean ± SEM from at least three independent experiments. See also Figure S5.

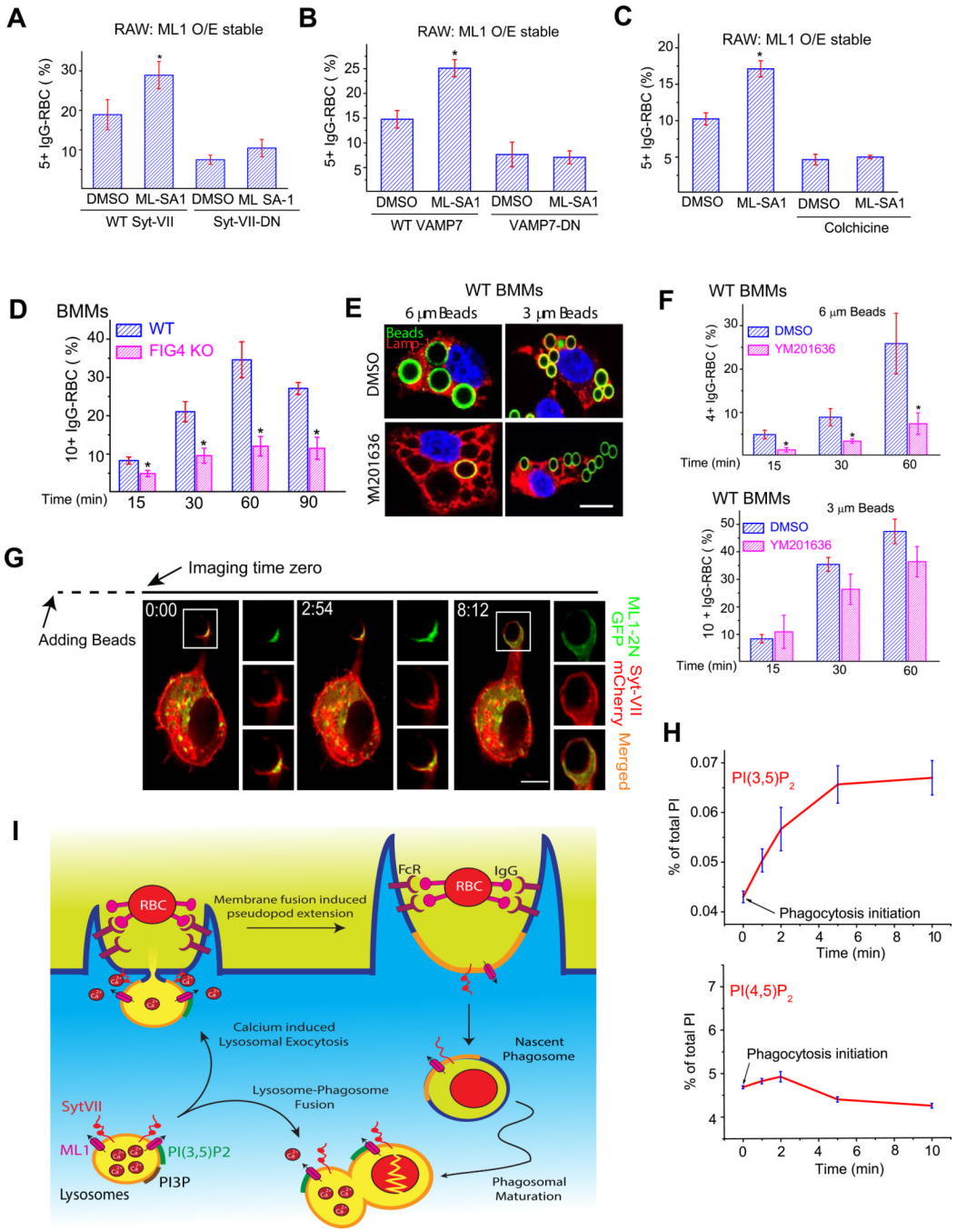

Figure 6. ML1-mediated facilitation of particle ingestion is dependent on lysosomal exocytosis

(A) ML-SA1 (10 μM) failed to increase particle ingestion in ML1 O/E RAW cells transfected with a Syt VII dominant-negative (DN) construct. Cells were pre-incubated with DMSO or ML-SA1 for 15 min before they were exposed to IgG-RBCs for 30 min. **(B)** ML-SA1 (10 μM) failed to increase particle ingestion in ML1 O/E RAW cells transfected with a VAMP7 dominant-negative (VAMP7-DN) construct. **(C)** A microtubule-disrupting agent colchicine (10 μM) inhibited ML-SA1-enhanced particle ingestion in WT BMMs. **(D)** FIG4 KO macrophages were defective in IgG-RBC ingestion. WT and FIG4 KO BMMs were exposed to IgG-RBCs for time periods indicated. **(E, F)** YM0201636 (1 μM for 2 hrs)

treatment inhibited uptake of 6 μm beads, but not 3 μm beads in WT BMMs. **(G)** Upon particle binding, ML1-2N-GFP and Syt VII-mCherry accumulated at the site of uptake within minutes (see Video 4). Note that phagocytosis initiation may have occurred before the imaging time zero due to a technical difficulty in identifying macrophages undergoing phagocytosis. **(H)** HPLC analysis of the levels of $PI(3,5)P_2$ and $PI(4,5)P_2$ during phagosome formation. Myo-[2-^{3}H] inositol-labeled RAW cells were exposed to IgG-coated beads (6 μm) for 0, 1, 2, 5, and 10 min at 37°C. At each time point, cells were centrifuged at 4°C and prepared for HPLC analysis. Data were from three independent experiments. **(I)** Particle binding activates lysosomal ML1 to initiate Ca^{2+}-dependent lysosomal exocytosis. Upon particle (IgG-RBC) binding, the activity of PIKfyve/Fab1 (not shown) is stimulated at the site of particle uptake. The subsequent increase of $PI(3,5)P_2$ level can then activate lysosomal ML1 to induce lysosomal Ca^{2+} release. Juxtaorganellar Ca^{2+} can then bind the Ca^{2+} sensor Syt VII to trigger lysosome-plasma membrane fusion, which provides substantial amount of lysosomal membranes for the pseudopod extension around IgG-RBCs. As a result, lysosomal membrane proteins, such as ML1 and Syt-VII, are inserted into the plasma membrane. Pseudopod extension continues until the IgG-RBCs are completely internalized. Phagocytic cups are then closed, and nascent phagosomes are formed. Newly formed phagosomes then undergo a series of membrane fusion and fission processes, collectively called phagosome maturation, to become late phagosomes. Lysosomes are also delivered to the late phagosomes through late phagosome maturation (phagosome-lysosome fusion), which is required for the degradation of phagocytic materials. ML1 may also plays a role in phagosome-lysosome fusion, however this requires further investigation. For all panels, unless otherwise indicated, the data represent the mean ± SEM from at least three independent experiments; 150–200 macrophages were analyzed for each experiment. For all panels, scale bars = 10 μm. See also Figure S6.

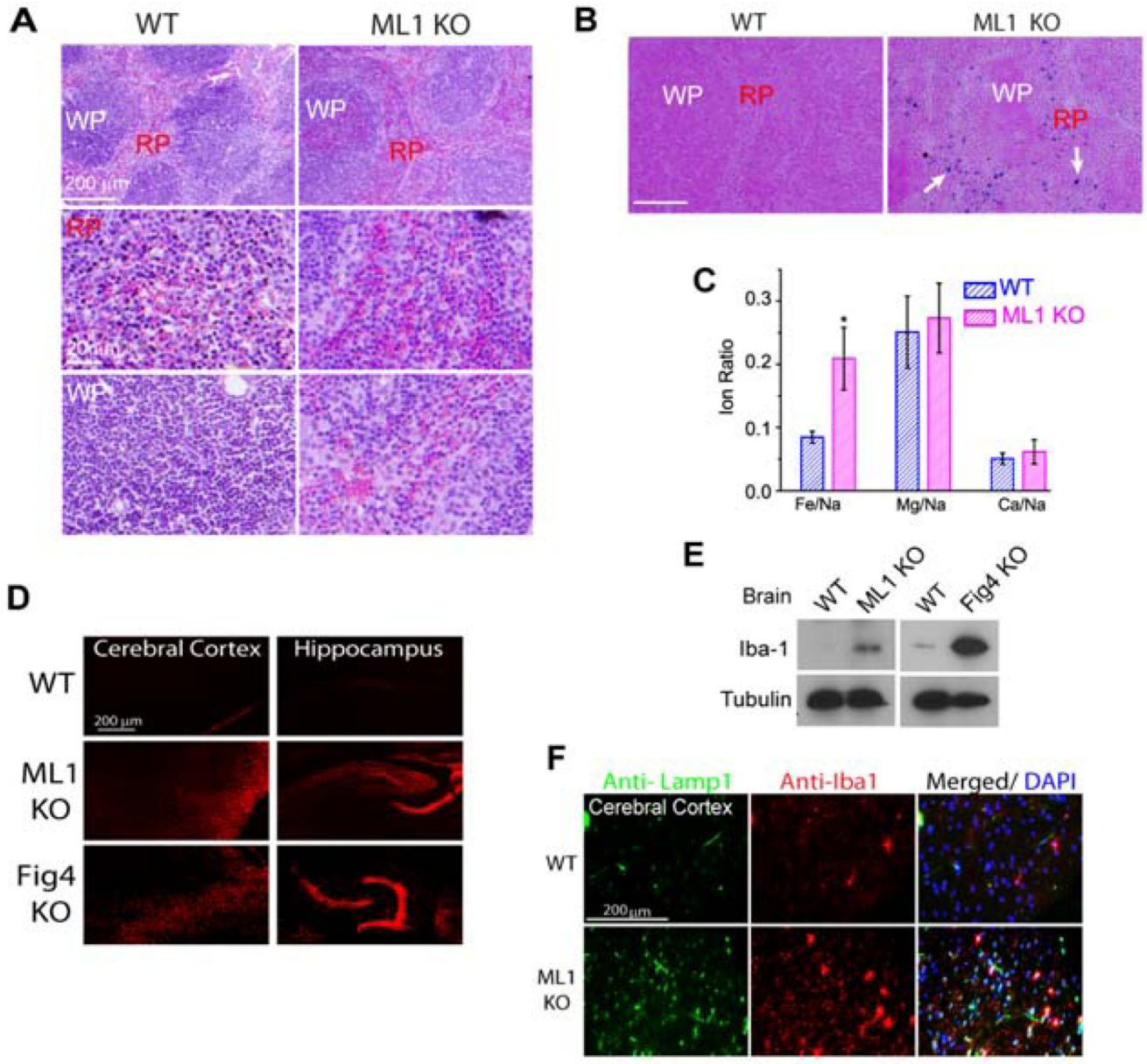

Figure 7. ML1 deficiency results in defective clearance of senescent red blood cells in the spleen and microglia activation in the brain

(A) Accumulation of RBCs in the red (RP) and white (WP) pulps of a ML1 KO spleen revealed by H&E staining. **(B)** Perl's (Prussian blue) staining for ferric iron in the splenic red pulp (RP) from 4-month-old mice. Scale bar = 200 μm. **(C)** ICP-MS analysis of the splenic iron content using digested whole spleens from WT and ML1 KO mice. Data were presented as ratios of different ions. **(D)** Propidium iodide (PI, 20 μg/ml) -labeled cells in the cerebral cortex and hippocampus of WT, ML1 KO, and FIG4 KO mouse brain sections. **(E)** Iba1 was up-regulated in the whole-brain lysates of ML1 and FIG4 KO mice. **(F)** Iba1-positive cells were up-regulated in the sections of the brain cortex of ML1 KO mice. For all panels, unless otherwise indicated, the data represent the mean ± SEM from at least three independent experiments. See also Figure S7.